Original Article

Carbon Chain Length Determines Inhibitory Potency of Perfluoroalkyl Sulfonic Acids on Human Placental 3β-Hydroxysteroid Dehydrogenase 1: Screening, Structure-Activity Relationship, and *In Silico* Analysis

TANG Lu Ming[1,&], MAO Bai Ping[2,&], ZHANG Bing Ru[2,&], LI Jing Jing[2], TANG Yun Bing[3], LI Hui Tao[2,3], and GE Ren Shan[2,4,#]

1. Department of Emergency Medicine, The Second Affiliated Hospital and Yuying Children Hospital of Wenzhou Medical University, Wenzhou 325000, Zhejiang, China; 2. Department of Anesthesiology, The Second Affiliated Hospital and Yuying Children Hospital of Wenzhou Medical University, Wenzhou 325000, Zhejiang, China; 3. Department of Obstetrics and Gynecology, The Second Affiliated Hospital and Yuying Children Hospital of Wenzhou Medical University, Wenzhou 325000, Zhejiang, China; 4. Key Laboratory of Structural Malformations in Children of Zhejiang Province, Wenzhou 325000, Zhejiang, China

Abstract

Objective This study aimed to compare 9 perfluoroalkyl sulfonic acids (PFSA) with carbon chain lengths (C4–C12) to inhibit human placental 3β-hydroxysteroid dehydrogenase 1 (3β-HSD1), aromatase, and rat 3β-HSD4 activities.

Methods Human and rat placental 3β-HSDs activities were determined by converting pregnenolone to progesterone and progesterone secretion in JEG-3 cells was determined using HPLC/MS–MS, and human aromatase activity was determined by radioimmunoassay.

Results PFSA inhibited human 3β-HSD1 structure-dependently in the order: perfluorooctanesulfonic acid (PFOS, half-maximum inhibitory concentration, IC_{50}: 9.03 ± 4.83 μmol/L) > perfluorodecanesulfonic acid (PFDS, 42.52 ± 8.99 μmol/L) > perfluoroheptanesulfonic acid (PFHpS, 112.6 ± 29.39 μmol/L) > perfluorobutanesulfonic acid (PFBS) = perfluoropentanesulfonic acid (PFPS) = perfluorohexanesulfonic acid (PFHxS) = perfluorododecanesulfonic acid (PFDoS) (ineffective at 100 μmol/L). 6:2FTS (1H, 1H, 2H, 2H-perfluorooctanesulfonic acid) and 8:2FTS (1H, 1H, 2H, 2H-perfluorodecanesulfonic acid) did not inhibit human 3β-HSD1. PFOS and PFHpS are mixed inhibitors, whereas PFDS is a competitive inhibitor. Moreover, 1–10 μmol/L PFOS and PFDS significantly reduced progesterone biosynthesis in JEG-3 cells. Docking analysis revealed that PFSA binds to the steroid-binding site of human 3β-HSD1 in a carbon chain length-dependent manner. All 100 μmol/L PFSA solutions did not affect rat 3β-HSD4 and human placental aromatase activity.

Conclusion Carbon chain length determines inhibitory potency of PFSA on human placental 3β-HSD1 in a V-shaped transition at PFOS (C8), with inhibitory potency of PFOS > PFDS > PFHpS > PFBS = PFPS = PFHxS = PFDoS = 6:2FTS = 8:2FTS.

Key words: 3β-hydroxysteroid dehydrogenase 1; Docking analysis; Perfluorooctanesulfonic acid; Progesterone; Structure–activity relationship

Biomed Environ Sci, 2023; 36(11): 1015-1027 *doi: 10.3967/bes2023.132* *ISSN: 0895-3988*

www.besjournal.com (full text) *CN: 11-2816/Q*

[&]These authors contributed equally to this work.

[#]Correspondence should be addressed to GE Ren Shan, Tel: 86-12123278761, E-mail: renshan_ge@wmu.edu.cn

Biographical notes of the first authors: TANG Lu Ming, male, born in 1980, PhD, majoring in prevention and control of infectious disease; MAO Bai Ping, female, born in 1989, PhD, majoring in anesthesiology and prevention and control of infectious disease.

INTRODUCTION

Poly- and perfluoroalkyl substances (PFAS) have poly- or perfluoroalkyl chains. Owing to their unique stabilities and surface activities, PFAS are widely used in many industrial and consumer products. Structurally, PFAS have fluorinated alkyl chains and polar head groups, including carboxylic acids (PFCA), such as perfluoroheptanoic acid (PFHpA, C7) and perfluorooctanoic acid (PFOA, C8), or sulfonic acids (PFSA), such as perfluoroheptanesulfonic acid (PFHpS, C7) and perfluorooctanesulfonic acid (PFOS, C8), which have an additional sulfur atom than the identical carbon-chained PFCA. PFSA are structurally similar; however, the carbon chain length varies. The PFSA include perfluorobutanesulfonic acid (PFBS, C4), perfluoropentanesulfonic acid (PFPS, C5), perfluorohexanesulfonic acid (PFHxS, C6), perfluorodecanesulfonic acid (PFDS, C10), and perfluorododecanesulfonic acid (PFDoS, C12) (Figure 1). PFSA containing at least one perfluorocarbon atom and some hydrogen-containing carbons are referred to as polyfluoroalkyl substances, such as 1H, 1H, 2H, 2H-perfluorooctanesulfonic acid (6:2FTS) and 1H, 1H, 2H, 2H-perfluorodecanesulfonic acid (8:2FTS) (Figure 1)[1]. They are used for coating textiles, paper, and upholstery, and as reaction additives in various processes[2-4].

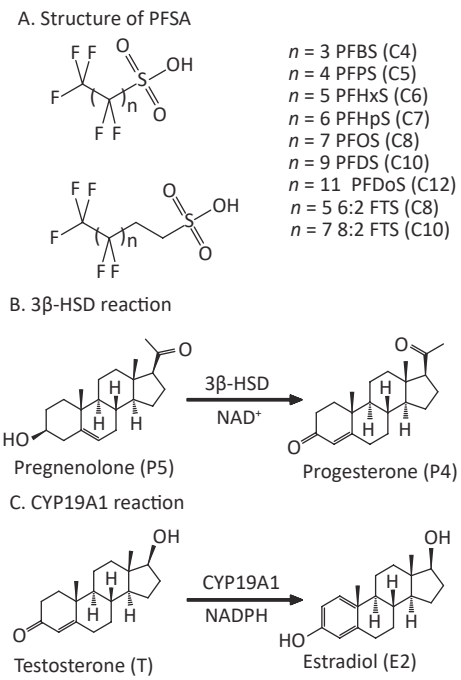

Figure 1. PFSA structure and placental 3β-HSD and CYP19A1 catalytic reactions. (A) Structure (*n* = number of carbon atoms); (B) 3β-HSD reaction; (C) CYP19A1 reaction. 3β-HSD, 3β-hydroxysteroid dehydrogenase; CYP19A1, aromatase; PFSA, polyfluoroalkyl sulfonic acid.

PFSA is widely present in the environment and the blood of the general population[5]. The average serum PFOS, PFOA, and PFHxS levels in the USA population were 14.7, 3.4, and 1.5 ng/mL[6]. Moreover, the PFOS level (33.3 ng/mL) in the population of two cities in northern China in 2012 was the highest, followed by PFHxS level (2.95 ng/mL)[7]. Serum PFOS levels may exceed 100 μg/mL in some factory workers[3]. PFOS and PFHxS persistently accumulate in the human body, and their serum elimination half-lives ($t_{1/2}$) are 5.4 and 8.5 years, respectively[8]. However, their serum elimination $t_{1/2}$ values are substantially lower in rats and monkeys[9]. Due to their high elimination $t_{1/2}$ and the potential persistent hazards in humans, 3M Company, a major PFAS manufacturer, has automatically phased out PFOS and PFOA production at the beginning of this century[6]. Short-chain PFSA compounds, such as PFBS and PFPS, have recently been introduced to replace PFOS and PFHxS because the serum elimination of PFBS is more rapid than that of PFOS and PFHxS. The $t_{1/2}$ of PFBS in male rats and monkeys is 3.1 and about 10 h, respectively[10].

PFAS act as endocrine disruptors. Human studies have established an association between PFOS level, preeclampsia, and low birth weights[11-14]. The adverse effects of PFAS may be associated with the interruption of steroid production in the human placenta. Progesterone (P4) and estradiol (E2) are steroid hormones secreted by the placenta and essential for maintaining pregnancy and fetal development. Human placental 3β-hydroxysteroid dehydrogenase/$\Delta^{5,4}$-isomerase 1 (*h*3β-HSD1) is a critical enzyme that catalyzes P4 biosynthesis from pregnenolone (P5) (Figure 1B). 3β-HSD1 sequence is highly similar to the rat homologue *r*3β-HSD4 in the placenta[15]. We have recently found that PFCA structure-dependently inhibited human placental *h*3β-HSD1 and *r*3β-HSD4, with perfluoroundecanoic acid (PFUA, C11) being the most potent inhibitor[16].

Aromatase (CYP19A1), an important enzyme in the placenta, is a cytochrome P450 enzyme and the rate-limiting enzyme in estrogen biosynthesis[17]. It catalyzes testosterone (T) conversion into E2 (Figure 1C). Estrogen synthesis in the placenta requires androgen from fetal and maternal adrenal glands, which produce large amounts of

dehydroepiandrosterone (DHEA) that enter the placenta[18]. In the human placenta, DHEA is converted by *h*3β-HSD1 into androstenedione, which is further converted into T by 17β-hydroxysteroiddehydrogenasesandthenE2byCYP19A1 (Figure 1C)[19]. Placental estrogen stimulates placental growth and enhances placental blood flow for the optimal exchange of gases and nutrients required for a rapidly developing fetus[20].

In this study, we explored the effects of nine PFSA molecules (C4–C12) on human placental *h*3β-HSD1, rat placental *r*3β-HSD4, and human placental CYP19A1 activity, as well as P4 production in human choriocarcinoma JEG-3 cells, and compared their potency, mode of action, and structure–activity relationship (SAR). We also performed docking analysis to determine the underlying mechanism.

MATERIALS AND METHODS

Chemicals and Animals

P5 (catalog #P9129), P4 (P0130), T (T-1500), E2 (E-8875), dimethyl sulfoxide (DMSO, D8418), NADPH (N7505), and NAD^+ (N7004) were purchased from Sigma–Aldrich (St. Louis, MO, USA). PFBS (C4, CAS#375-73-5, Cat#387933, purity 98%) was purchased from J&K Scientific (Beijing, China), PFHpS (C7, CAS#375-92-8, Cat#C15986880, purity 95.3%) and 8:2FTS (CAS#39108-34-4, Cat#C15986585, purity 95.3%) were purchased from Dr. Ehenstorfer (Augsburg, Germany), PFPS (C5, CAS#2706-91-4, Cat#ACM2706914, purity 96%) was purchased from Alfa Chemistry (Ronkonkoma, NY, USA), PFOS (C8, CAS#1763-23-1, Cat#H0781, purity 98%) was purchased from TCI (Tokyo, Japan), PFHxS (C6, CAS#355-46-4, Cat#P999738, purity 98%) and PFDS (C10, CAS#335-77-3, Cat#P286540, purity 95%) were purchased from TRC (Toronto, Canada), 6:2FTS (C10, CAS#27619-97-2, Cat#T923214, purity 98%) was purchased from Macklin (Shanghai, China), PFDoS (C12, CAS#1260224-54-1, Cat#1ST14848, purity 98%) was purchased from Alta Scientific (Tianjin, China). PFSA compounds were dissolved in DMSO. Pregnant Sprague-Dawley rats (280–320 g) were obtained from the Shanghai Laboratory Animal Center (Shanghai, China). Rat placentas were obtained from dams on gestational day 20 after the rats were euthanized by CO_2 and cervical dislocation. The Animal Care and Use Committee of Wenzhou Medical University approved all animal protocols. The Second Affiliated Hospital of Wenzhou Medical University provided full-term human placental samples under the endorsement of the Hospital Ethics Committee and the subjects' agreement (Protocol no. 2022-K-81-01). The human choriocarcinoma cell line JEG-3 was obtained from the American Type Culture Collection (ATCC; Manassas, VA, USA).

Microsomal Preparation

Microsomes were prepared from the placenta at 4 °C as described previously[16]. Briefly, homogenized placental suspension in 0.01 mol/L phosphate-buffered saline (PBS, pH 7.2) supplemented with 0.25 mol/L sucrose was sequentially centrifuged at 700 ×*g* for 30 min, 14,500 ×*g* for 30 min, and then 105,000 ×*g* twice for 1.5 h for obtaining the microsomal pellet, which was resuspended in ice-cold PBS, and its protein content was measured by an enhanced BCA protein assay kit (Cat#P0010, Beyotime Biotech; Shanghai, China) according to the manufacturer's instruction.

3β-HSD Assay

Both human *h*3β-HSD1 and rat *r*3β-HSD4 catalyze P5 conversion to P4, which can be measured using the HPLC/MS–MS method[16]. The following operations were performed: 1) a linear reaction condition for 3β-HSD was established after incubating the assay system (a 1.5 mL tube containing 200 nmol/L P5, 200 μmol/L NAD^+, and 5 μg placental microsome in 100 μL pH 7.2 0.01 mol/L PBS) for 0–90 min in a shaking water bath (75 rpm) at 37 °C; 2) Michaelis–Menten kinetics of each enzyme was established after incubating the assay system (a 1.5 mL tube containing 0–2 μmol/L P5, 200 μmol/L NAD^+, and 5 μg placental microsome in 100 μL 0.01 mol/L PBS) for 60 min; 3) a screening test for PFSA-mediated 3β-HSD inhibition was established after incubating the assay system (a 1.5 mL tube containing 200 nmol/L P5, 200 μmol/L NAD^+, 5 μg placental microsome, and 100 μmol/L PFSA in 100 μL 0.01 mol/L PBS) for 60 min; 4) the dose response of each PFSA was measured after incubating the assay system (a 1.5 mL tube containing 200 nmol/L P5, 200 μmol/L NAD^+, 5 μg placental microsome, and 0–200 μmol/L PFSA 100 μL 0.01 mol/L PBS) for 60 min; 5) the enzyme kinetics inhibition assay was established after incubating the assay system (a 1.5 mL tube containing 0–5 μmol/L P5, 200 μmol/L NAD^+, 5 μg placental microsome, and 0–200 μmol/L PFSA in 100 μL 0.01 mol/L PBS) for 60 min. At the end of the reaction, 10 μL internal standard (IS, T-d5, Shanghai Zzbio Co., China) together with 200 μL acetonitrile (Merck Supelco,

PA) was added to the tube in an ice bath, and the tube was centrifuged at 20,000 ×*g* for 10 min. Then, 10 µL extract was injected into HPLC–MS/MS system for measuring P4 amount.

P4 Amount Determination Using HPLC–MS/MS

HPLC–MS/MS (Waters, USA) equipped with an Acquity BEH C18 column (2.1 mm × 50.0 mm, 1.7 µm particle size) was used to determine P4[16]. A gradient procedure in mixed solvent A (0.1% aqueous formic acid solution) and solvent D (acetonitrile) was programmed as follows: 70%–30% D (0–0.3 min), 10%–90% D (0.3–1.9 min), 70%–30% A (1.9–2.0 min). The flow rate was 0.40 mL/min and the injection volume was 10 µL. The column and sample temperatures were 30 and 4 °C, respectively. The XEVO TQD triple quadrupole mass spectrometer equipped with ESI source (Waters) was used for mass determination in a multiple-reaction monitoring mode and the MRM mode transitions for P4 and IS were m/z 315.16→96.92 and 289.07→ 96.92, respectively. Masslynx 4.1 (Waters) software was used for data acquisition and control. The P4 amount was calculated using the standard curve method with IS.

JEG-3 Cell Culture and Treatment

The JEG-3 choriocarcinoma cell line is widely used as a placental steroid production model[19]. This cell line is derived from a human choriocarcinoma, produces a substantial P4 amount, and contains *h*3β-HSD1 and CYP19A1[19]. Therefore, it was used as a placental syncytiotrophoblast model in this study. Briefly, 10^5 cells were cultivated per well in 24-well plates using Minimum Essential Medium (MEM) supplemented with phenol red, 10% fetal calf serum (FCS), and various PFOS and PFDS concentrations at 37 °C and 5% CO_2 for P4 production for 24 h. The media were collected for measuring P4 using HPLC–MS/MS method. For cytotoxicity analysis, the cells were treated with 100 µmol/L PFOS and PFDS and their viability was tested. For viability assay, 5,000 cells were seeded per well in 100 µL medium in 96-well plates and treated with 100 µmol/L PFOS and PFDS for 24 h. The optical density (OD) at 450 nm was measured using the Cell Counting Kit-8 (CCK-8, Sigma–Aldrich). Five samples were measured at each point and the results were averaged.

CYP19A1 Activity Assay

Human CYP19A1 catalyzes T to E2 conversion, which can be measured using a radioimmunoassay[21]. Briefly, the following operations were performed: 1) a linear reaction condition for CYP19A1 was established after incubating the assay system (a 1.5 mL tube containing 100 nmol/L T, 200 µmol/L NADPH, and 5 µg human placental microsome in 200 µL pH 7.2 0.01 mol/L PBS) for 0–120 min in a shaking water bath (75 rpm) at 37 °C; 2) Michaelis–Menten kinetics of CYP19A1 was established after incubating the assay system (a 1.5 mL tube containing 0–1 µmol/L T, 200 µmol/L NADPH, and 5 µg placental microsome in 200 µL 0.01 mol/L PBS) for 60 min; 3) a screening test for PFSA-mediated CYP19A1 inhibition was established after incubating the assay system (a 1.5 mL tube containing 100 nmol/L T, 200 µmol/L NADPH, 5 µg placental microsome, and 100 µmol/L PFSA in 200 µL 0.01 mol/L PBS) for 60 min. The reactions were terminated by adding 10 µL 1 N HCl. E2 amount in the reaction medium was measured using radioimmunoassay[21]. A standard curve was prepared using 10–2,000 pg/mL E2, the bound and free steroids were separated with a charcoal–dextran suspension, and radioactivity was determined using a β-counter (PE). The minimum detectable E2 amount was 5 pg/mL.

Dose Response and Enzyme Kinetics Inhibition Analysis

Dose response and mode of action (MOA) were analyzed as previously described[16]. Control (DMSO) activity was set at 100%. Residual activity after PFSA treatment was normalized to that of the control. When the residual activity after PFSA treatment was less than or equal to 50%, the half-maximum inhibitory concentration (IC_{50}), which was calculated from the nonlinear regression (curve fit) of the dose response inhibition model, in which the inhibitor and response (three parameters) were calculated using GraphPad (GraphPad Inc., CA, USA). For MOA, enzyme kinetics inhibition (mixed model) with the following equations were used:

$$V_{maxApp} = \frac{V_{max}}{1 + \frac{I}{\alpha \times K_i}} \quad (1)$$

$$K_{mApp} = K_m \times \frac{1 + \frac{I}{K_i}}{1 + \frac{I}{\alpha \times K_i}} \quad (2)$$

$$Y = \frac{V_{maxApp} \times X}{K_{mApp} + X} \quad (3)$$

where V_{max} is the maximum velocity (pmol·mg^{-1}·min^{-1}), I is the inhibitor concentration, K_i is the inhibition constant, K_m is Michaelis–Menten kinetics constant, and α is a factor to judge the MOA. "α = 1" indicates noncompetitive inhibition, "α > 1 or < 1" indicates mixed inhibition, "α near 0 but not equal to 0" indicates uncompetitive inhibition; "α > ∞" indicates competitive inhibition. A Lineweaver–Burk plot (LBP) was drawn after comparing 1/V (velocity) with 1/substrate concentration (1/[P5]) to further evaluate the MOA of PFSA.

Molecular Simulation Analysis for PFSA with h3β-HSD1

AlphaFold human *h*3β-HSD1 model (AF-P14060-F1-model) [https://alphafold.ebi.ac.uk/entry/P14060][22,23], with 94.16 average model confidence (pLDDT), was selected as the human *h*3β-HSD1 target for *in silico* docking analysis. PFSA was sketched in ChemBioDraw Ultra 12.0 (Cambridge, UK) in the mol2 format. Docking analysis was performed with SwissDock web Server[24], and the lowest binding energy was calculated and visualized by Chimera 1.1.1 software (San Francisco, CA, USA). Hydrogen bonds and amino acid residues were labeled using a chimera. PyMOL software was used for the 3D structure and measurement of the chemical length. 2D graphics of the superimposed structures of PFSA with P5 were analyzed using LigPlot[25].

Statistics

The assays were repeated 4–8 times. Enzymatic results were analyzed using one-way ANOVA followed by *post hoc* Tukey's multiple comparisons to identify significant differences between the groups for the screening test. Significant differences are denoted as $^{*}P < 0.05$, $^{**}P < 0.01$, $^{***}P < 0.001$, $^{\$}P < 0.05$, and $^{\$\$\$}P < 0.001$. Data are presented as means ± standard deviation (SD).

RESULTS

PFSA Structure-Dependently Inhibit h3β-HSD1 Activity

Time-dependent *h*3β-HSD1 activity was measured after mixing 200 nmol/L P5 and 0.2 mmol/L NAD^+ with human placental microsome for 0–90 min. P5 to P4 conversion rate was linear within 90 min (Figure 2A). When 0–2 μmol/L P5 was incubated with 0.2 mmol/L NAD^+ and 5 μg human placental microsome for 60 min, the K_m and V_{max} for *h*3β-HSD1 were 0.228 ± 0.053 μmol/L and 1.152 ± 0.044 nmol·mg^{-1}min^{-1}, respectively (Figure 2B), which is within the previously reported range[26]. The screening results showed that PFHpS, PFOS, and PFDS significantly inhibited *h*3β-HSD1 activity, resulting in residual activity close to or lower than 50% of the control activity (Figure 2C). Although PFOS and 6:2FTS have the same number of carbon atoms, 100 μmol/L 6:2FTS did not inhibit *h*3β-HSD1 activity. This was also true for 8:2FTS and PFDS (Figure 2C). These results indicate that PFSA structure-dependently inhibits *h*3β-HSD1 activity. The dose response of PFSA molecules with approximately 50% or lower residual activity than control was determines using a concentration series. The IC_{50} of PFOS, PFDS, and PFHpS were 9.03 ± 4.82, 42.52 ± 8.99, and 112.6 ± 29.39 μmol/L, respectively (Table 1 and Figure 2D–F). The enzyme kinetics inhibition analysis revealed that the K_i of PFOS, PFDS, and PFHpS were 8.32, 43.41, and 114.7 μmol/L, respectively (Table 1 and Figure 3). These results indicate that the inhibitory potency is PFOS > PFDS > PFHpS > PFBS = PFPS = PFHxS = PFDoS for *h*3β-HSD1, showing a V-shaped turn at PFOS (C8). Enzyme kinetics inhibition (mixed model) and Lineweaver–Burk plot analysis showed that PFOS and PFHpS were mixed inhibitors, whereas PFDS was a competitive P5 inhibitor (Figure 3 and Table 1).

Docking Analysis of PFSA with h3β-HSD1

3D *h*3β-HSD1 structure (AF-P14060-F1) constructed using AlphaFold2 was used. P5 docked to *h*3β-HSD1. Docking revealed that P5 forms two hydrogen bonds with *h*3β-HSD1 catalytic residues, Ser125 and Tyr155 (Figure 4A), and contacts 13 residues (Val88, Ser125, Ile126, Glu127, Tyr155, Pro187, Met188, Tyr189, Ile190, Phe197, Tyr265, Ile319, and Leu322) (Figure 4B). This is consistent with the results of a previous docking model by Autodock for *h*3β-HSD1 with catalytic residues Ser124 and Tyr154, because it lacks one amino acid[27]. All PFSA were docked to the steroid-binding active site of *h*3β-HSD1. PFOS contacts five residues (Table 2), overlaps with four substrate-binding residues, and forms two hydrogen bonds (Figure 4C and 4D), and the lowest binding energy is −7.272 kcal/mol (Table 1). PFDS contacts eight residues (Table 2), overlaps with six substrate-binding residues, and forms one hydrogen bond with residue Tyr155 (Figure 4E and 4F), and the lowest binding energy is −7.153 kcal/mol (Table 1). PFHpS contacts 11 residues (Table 2), overlaps with six substrate-

binding residues, and forms three hydrogen bonds (Figure 4G and 4H); the lowest binding energy was −6.800 kcal/mol (Table 1). Interestingly, the lowest binding energy values of other PFSA molecules were greater than −6.800 kcal/mol (Table 1), although they overlap with more than three substrate-binding residues (Supplementary Figure S1, available in www.besjournal.com). FTS connect with several substrate-binding residues and form hydrogen bonds with the catalytic residue Tyr155. However, the hydrogen atoms near the sulfonic acid moiety, instead of those near the fluorine atoms, may cause

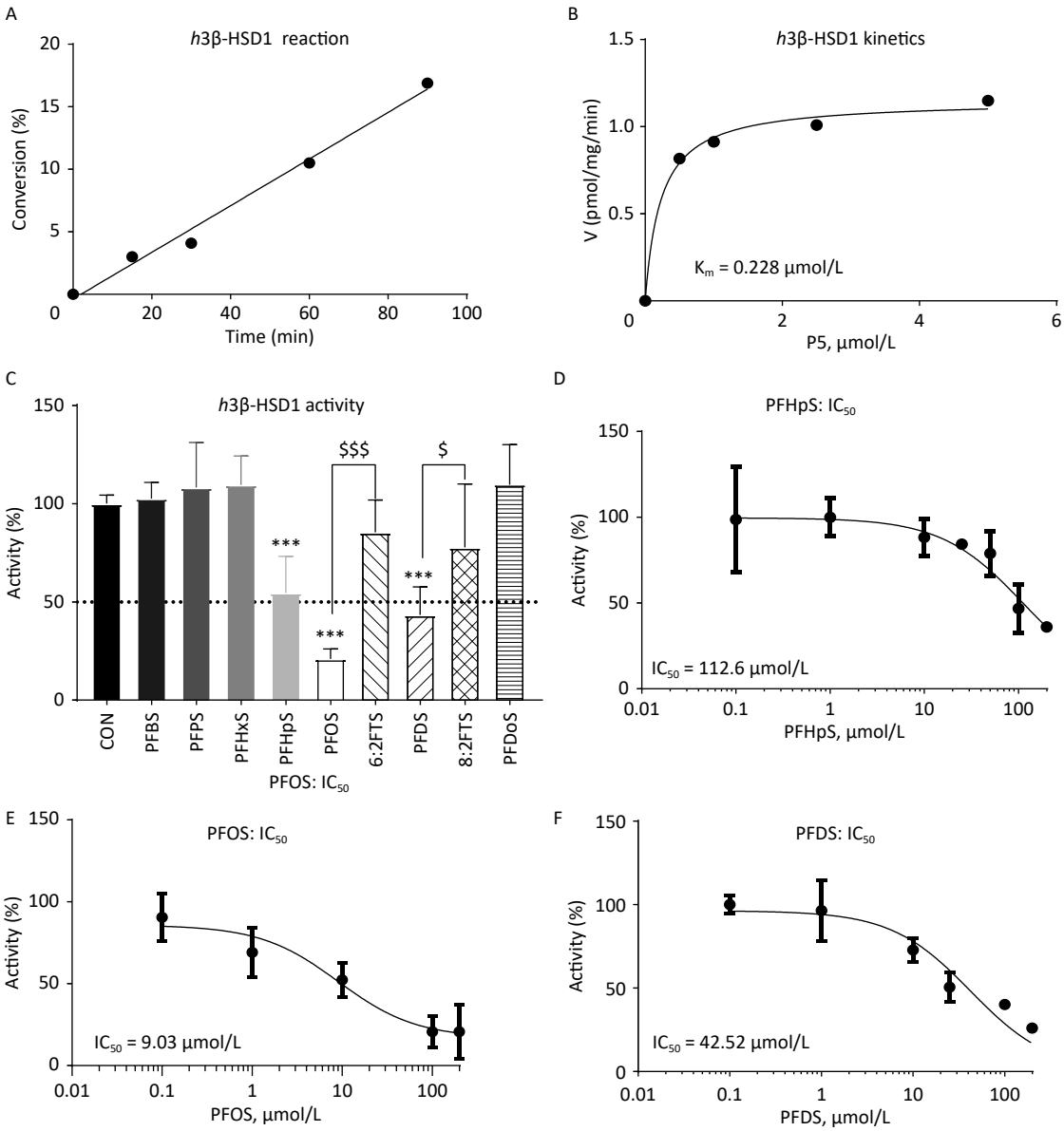

Figure 2. Time-curve reaction, Michaelis–Menten kinetics, screening assay, and dose response of PFSA to inhibit placental *h*3β-HSD1 activity. (A) Time-curve reaction; (B) Michaelis–Menten kinetics; (C) Screening for PFSA to inhibit human placental *h*3β-HSD1 activity: means ± SD (n = 4–8); ***Indicates significant difference compared to CON at $P < 0.001$, $^{\$\$\$}$PFOS *vs.* 6:2FTS at $P < 0.001$, $^{\$}$PFDS *vs.* 8:2FTS at $P < 0.05$; (D–F) IC_{50} of PFHpS, PFOS, and PFDS, respectively. 6:2FTS, 1H, 1H, 2H, and 2H-perfluorooctanesulfonic acid; 8:2FTS, 1H, 1H, 2H, and 2H-perfluorodecanesulfonic acid; CON, control; *h*3β-HSD1, human 3β-hydroxysteroid dehydrogenase 1; IC_{50}, half-maximum inhibitory concentration; PFDS, perfluorodecanesulfonic acid; PFHpS, perfluoroheptanesulfonic acid; PFOS, perfluorooctanesulfonic acid; PFSA, polyfluoroalkyl sulfonic acid; SD, standard deviation.

less negative attraction with *h*3β-HSD1, which may decrease the binding affinity (Supplementary Figure S1). The short-chain PFSA molecules, (such as PFBS), are extremely small, possibly decreasing the binding affinity (Supplementary Figure S2, available in www.besjournal.com). We further measured the molecular length of P5 and each PFSA, and found that the appropriate molecular length of P5, PFOS, PFBS, and PFDoS are 12, 11.6, 7.1, and 16.7 Å, respectively. We calculated the correlation between the K_m of P5, K_i of PFHpS and PFOS, the molecular size, and the correlation between K_i and the lowest binding energy of PFHpS, PFOS, and PFDS. K_i/K_m were inversely correlated with P5, PFHpS, and PFOS size (Figure 5A, R^2 = 0.978), indicating that PFHpS and PFOS inhibit human 3β-HSD1, and K_i positively correlates with the lowest binding energy (Figure 5B, R^2=0.993). This indicates that PFSA size should match the binding cavity like substrate P5 (12 Å), and lowest binding energy can well predict the inhibitory potency of PFSA.

PFOS and PFDS Inhibit P4 Production in JEG-3 Cells

To test whether PFOS and PFDS can inhibit P4 synthesis, JEG-3 cells were treated with 1–100 μmol/L PFOS and PFDS, where the highest concentration (100 μmol/L) was based on the highest serum PFSA levels (114.1 mg/L, 100–250 μmol/L PFOS) in occupational workers[28]. We found that ≥ 1 μmol/L PFOS significantly decreased P4 output and 10–100 μmol/L PFDS significantly reduced P4 levels (Figure 6). These results indicated that PFOS and PFDS can inhibit P4 biosynthesis.

PFSA Do not Affect Rat Placental r3β-HSD4 Activity

Rat placental *r*3β-HSD4 is a human placental *h*3β-HSD1 homologue that is highly similar to human *h*3β-HSD1[15]. Previous studies have shown that some PFAS molecules, such as perfluoroundecanoic acid (PFUnA), inhibit rat *r*3β-HSD4 activity[16]. Michaelis–Menten kinetics analysis showed that the K_m and V_{max} of *r*3β-HSD4 were 0.228 ± 0.078 μmol/L and 37.38 ± 4.06 pmol/mg/min, respectively, (Figure 7A), and the K_m is similar to the previously reported value[15]. We screened the inhibitory effect of 100 μmol/L PFSA on *r*3β-HSD4. None of the PFSA tested inhibited rat 3β-HSD4 (Figure 7B), indicating species-dependent difference in placental 3β-HSD inhibition.

PFSA Do not Affect Human Placental CYP19A1 Activity

Human placental CYP19A1 catalyzes E2 formation from T. Michaelis–Menten kinetics analysis showed that the K_m and V_{max} of human placental CYP19A1 were 0.183 ± 0.053 μmol/L and 66.81 ± 6.63 $pmol \cdot mg^{-1} \cdot min^{-1}$, respectively (Figure 8A), and the K_m is similar to the previously

Table 1. Information of PFSA to inhibit human 3β-HSD1

Name	Length (Å)	IC_{50} (μmol/L)	K_i/K_m (μmol/L)	LBE, (kcal/mol)	Mode action	Binding site
P5	12.0	ND	0.308	−8.754	competitive	Steroid
PFBS (C4)	7.2	NI	ND	−6.620	ND	Steroid
PFPS (C5)	8.9	NI	ND	−6.320	ND	Steroid
PFHxS (C6)	9.9	NI	ND	−6.555	ND	Steroid
PFHpS (C7)	10.2	112.6 ± 29.39	114.7	−6.800	ND	Steroid
PFOS (C8)	11.6	9.03 ± 4.83	8.32	−7.272	mixed	Steroid
6:2FTS (C8)	12.0	NI	ND	−6.661	ND	Steroid
PFDS (C10)	14.4	42.52 ± 8.99	43.41	−7.153	competitive	Steroid
8:2FTS (C10)	14.4	NI	ND	−6.709	ND	Steroid
PFDoS (C12)	16.7	NI	ND	−6.531	ND	Steroid

Note. IC_{50} = half-maximal inhibitory concentration, K_i = measured inhibition constant, LBE = lowest binding energy; NI = No inhibition at 100 μmol/L; ND = Not determined. IC_{50}, half-maximum inhibitory concentration; PFBS, perfluorobutanesulfonic acid; PFDS, perfluorodecanesulfonic acid; PFHpS, perfluoroheptanesulfonic acid; *h*3β-HSD1, human 3β-hydroxysteroid dehydrogenase 1; PFHpS, perfluoroheptanesulfonic acid; PFHxS, perfluorohexanesulfonic acid; PFOS, perfluorooctanesulfonic acid; PFDoS, perfluorododecanesulfonic acid; 6:2FTS, 1H, 1H, 2H, and 2H-perfluorooctanesulfonic acid; 8:2FTS, 1H, 1H, 2H, and 2H-perfluorodecanesulfonic acid; SD, standard deviation.

reported value [21]. We screened the inhibitory effect of 100 μmol/L PFSA on human placental CYP19A1. None of the PFSA tested inhibited human CYP19A1 (Figure 8B), indicating that PFSA specifically inhibits human placental 3β-HSD1 activity.

DISCUSSION

This study shows that PFSA molecules structure-dependently inhibit human placental *h*3β-HSD1 activity in the order PFOS > PFDS > PFHpS > PFBS = PFPS = PFHxS = PFDoS = 6:2FTS = 8:2FTS. Since *h*3β-HSD1 is critical for P4 biosynthesis in the human placenta, some PFSA molecules may disrupt placental function by directly inhibiting *h*3β-HSD1 activity.

We have previously shown that inhibitory potency gradually increased in C9–C11 PFCA molecules, showed a V-shaped transition, and gradually lost in C11–C14 molecules[16]. Interestingly, we also observed this phenomenon in the PFSA subclass in this study: some PFSA from inhibitory potency gradually increased in PFHpS (C7) to PFOS (C8), followed by a V-shaped transition, and gradually lost in C8 to PFDoS (C12). However, the structure-dependent inhibition between PFCA and PFSA subclasses is slightly different: in PFCA subclass, 100 μmol/L PFHpA (C7) and PFOA (C8) did not inhibit

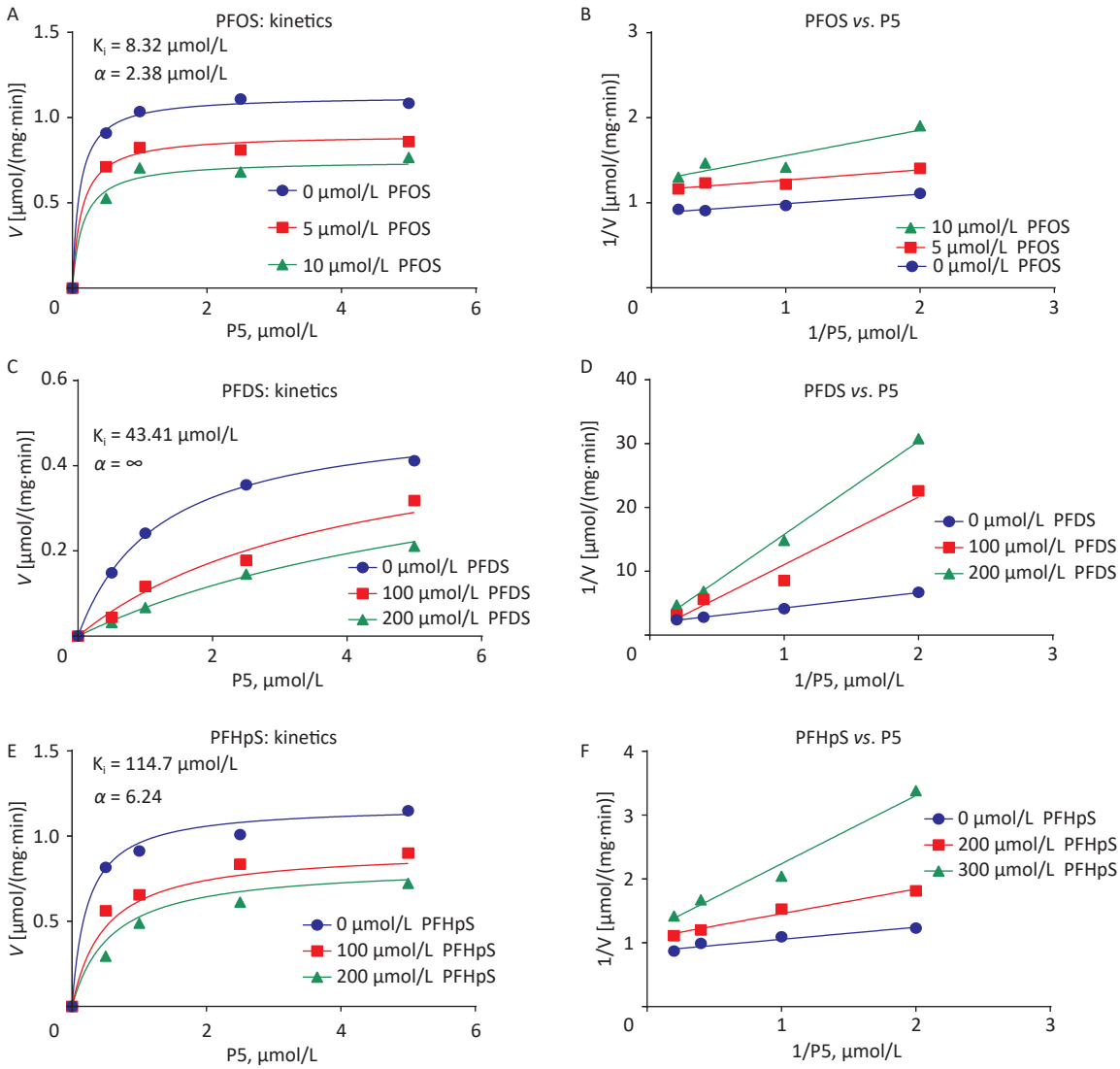

Figure 3. (A, C, E) Enzyme kinetics inhibition and (B, F, F) Lineweaver–Burk plot analysis for mode of action of PFOS, PFDS, and PFHpS. PFDS, perfluorodecanesulfonic acid; PFHpS, perfluoroheptanesulfonic acid; PFOS, perfluorooctanesulfonic acid.

*h*3β-HSD1 activity as previously reported[16], while in the PFSA subclass, 100 μmol/L PFHpS (C7) and PFOS (C8) significantly inhibited this enzyme activity (this study). These results indicate that the extra sulfur atom extends the carbon chain length and different functional groups (such as sulfonic acid in PFSA) change the inhibitory pattern.

Previous studies showed that *h*3β-HSD1 contains critical three catalytic residues: Ser124, Tyr154, and Lys158[27]. Due to the extra amino acids in our *h*3β-HSD1 model, our docking analysis showed that the catalytic residues of *h*3β-HSD1 are Ser125, Tyr155, and Lys159, and that P5 forms two hydrogen bonds with Ser125 and Tyr155, confirming Thomas's model prepared using Autodock[27]. The molecular length of P5 is 12 Å. Docking analysis showed that all PFSA bound to the active site of the steroid-binding cavity of *h*3β-HSD1. However, the lowest binding affinity differs depending on the carbon chain length, additional sulfur atoms, and functional groups (sulfonic acid). The binding affinity gradually increased in C4–C8 PFSA molecules, as judged by the lowest binding energy, indicating that the inhibitory potency increased with size. However, the binding affinity gradually decreased in C8–C12 PFSA molecules, as judged by the lowest binding energy, indicated a decrease in inhibitory potency, leading to a V-shaped turn. The molecular length of PFSA, due to carbon and sulfur atom number, should be adequate to occupy the catalytic cavity for maximum binding with *h*3β-HSD1. Short-chain PFSA molecules, such as PFBS (7.2 Å), are small for significant hydrophobic interactions with *h*3β-HSD1 (Supplementary Figure S2). Long-chain PFSA molecules, such as PFDoS (16.7 Å), are easily stretched out from the catalytic cavity to form hydrophobic interactions with the catalytic residues of *h*3β-HSD1 (Supplementary Figure S2). PFOS molecule is 11.6 Å long, approximating the molecular length of substrate P5 (12.0 Å). This may explain why PFOS was the most potent PFSA to inhibit *h*3β-HSD1. Interestingly, 6:2FTS and 8:2FTS were ineffective than their analogs, PFOS and PFDS, although 6:2FTS and PFOS had the same number of carbon atoms and sulfonic acid group, and 8:2FTS and PFDS had the same number of carbon atoms and sulfonic acid group. Both 6:2FTS and P5 are 12 Å molecules, indicating that 6:2FTS may not have more negative charges from additional fluorine atoms compared to PFOS to form enough affinity. This could also be true for 8:2FTS.

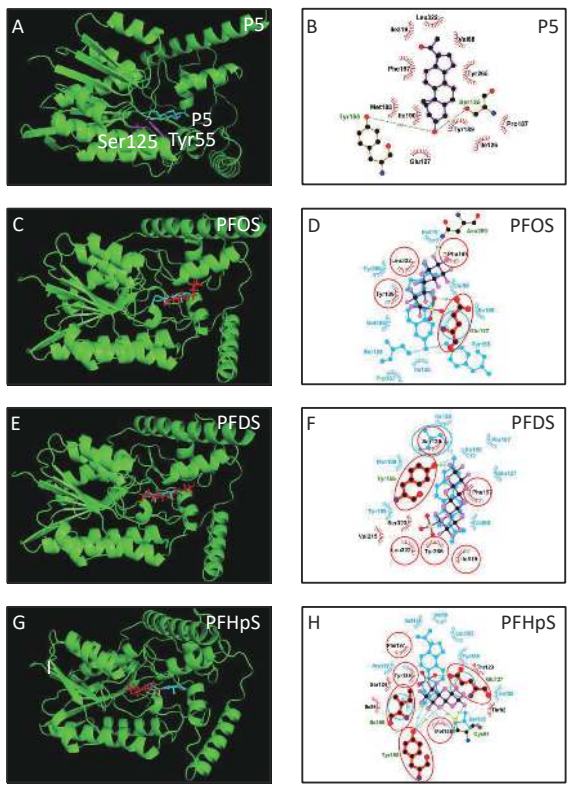

Figure 4. *In silico* analysis of perfluoroalkyl sulfonic acid with *h*3β-HSD1. The 3D model of *h*3β-HSD1 contains the catalytic residues Ser125 and Tyr155 (pink in A). (A, C, E, G) 3D structure of P5 (cyan), PFOS (red), PFDS (red), PFHpS (red), respectively; (B) 2D for P5; (D, F, H) superimposed images for PFOS (purple), PFDS (purple), PFHpS (purple): hydrogen bonds (green line), overlapping residues (red circled), P5 (cyan) as background. *h*3β-HSD1, human 3β-hydroxysteroid dehydrogenase 1; P5, pregnenolone; PFDS, perfluorodecanesulfonic acid; PFHpS, perfluoroheptanesulfonic acid; PFOS, perfluorooctanesulfonic acid.

Moreover, some PFAS can inhibit testicular *h*3β-HSD2, an *h*3β-HSD1 isoform[29]. Although *h*3β-HSD1 and *h*3β-HSD2 protein sequences are highly similar (93.6%)[30], they showed different sensitivity toward PFAS[29]. PFOS potently inhibits *h*3β-HSD1 (in this study), but did not affect *h*3β-HSD2 activity[29], indicating that *h*3β-HSD1 and *h*3β-HSD2 have different secondary structures.

PFAS also suppresses several hydroxysteroid dehydrogenase activities structure-dependently: PFOS > PFHxS = PFBS in inhibiting testicular *r*3β-HSD1 and human testicular 17β-hydroxysteroid dehydrogenase 3[29]; PFOS > PFHxS > PFBS in inhibiting human 11β-hydroxysteroid dehydrogenase 2; PFOS > PFHxS > PFBS in inhibiting rat 11β-

Table 2. Contacting residues, hydrogen (H) bonds, and overlapping residues of PFSA with pregnenolone to human 3β-HSD1

Compd.	Contacting residues	H bonds	Overlapping residues
PFBS	Ile86, Glu127, Tyr155, Val88, Tyr189, Ile190, Phe197, Leu322	Glu127(3.27Å), Tyr155(2.76Å)	Val88, Glu127, Tyr155, Tyr189, Ile190, Phe197, Leu322
PFPS	Ile86, Val88, Glu127, Tyr189, Phe197, Leu322	Glu127(2.84Å)	Val88, Glu127, Tyr189, Phe197, Leu322
PFHxS	Ile86, Val88, Glu127, Phe197	Glu127(2.71Å)	Val88, Glu127, Phe197
PFHpS	Thr82, Cys84, Ile86, Thr 123, Ser124, Glu127, Tyr155, Met188, Tyr189, Ile190, Phe197	Cys84(3.01Å), Tyr155(2.88Å), Glu127(2.88Å), Ile190(2.92Å)	Glu127, Tyr155, Met188, Tyr189, Ile190, Phe197
PFOS	Glu127, Tyr189, Phe197, Asn269, Leu322	Glu127(2.78Å), Asn269(3.32Å)	Glu127, Tyr189, Phe197, Leu322
6:2FTS	Glu127, Ser125, Tyr155, Met188, Tyr189, Ile190, Phe197	Tyr155(2.80Å)	Glu127, Ser125, Tyr155, Met188, Tyr189, Ile190, Phe197
PFDS	Ser125, Tyr155, Phe197, Val215, Tyr265, Ile319, Ser323, Leu322	Tyr155(2.78Å),	Ser125, Tyr155, Phe197, Tyr265, Ile319, Leu322
8:2FTS	Ser124, Ser125, Tyr155, Tyr189, Ile190, Phe197, Tyr265, Leu322	Ser155(2.89Å), Tyr155(3.00Å),	Ser125, Tyr155, Tyr189, Ile190, Phe197, Tyr265, Leu322
PFDoS	Ile86, Ser125, Glu127, Tyr155, Tyr189, Ile190, Phe197, Ans269, Leu322	Asn269(3.00Å)	Ser125, Glu127, Tyr155, Tyr189, Ile190, Phe197, Ans269, Leu322

Note. PFBS, perfluorobutanesulfonic acid; PFDS, perfluorodecanesulfonic acid; PFHpS, perfluoroheptanesulfonic acid; h3β-HSD1, human 3β-hydroxysteroid dehydrogenase 1; PFHpS, perfluoroheptanesulfonic acid; PFHxS, perfluorohexanesulfonic acid; PFOS, perfluorooctanesulfonic a.

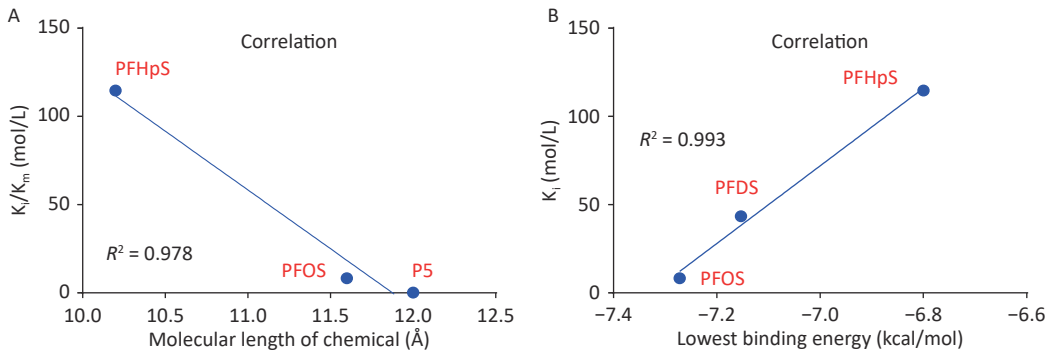

Figure 5. Correlation between K_i and (A) molecular length of P5 and perfluoroalkyl sulfonic acid and (B) lowest binding energy. K_i, inhibition constant; P5, pregnenolone; PFDS, perfluorodecanesulfonic acid; PFHpS, perfluoroheptanesulfonic acid.

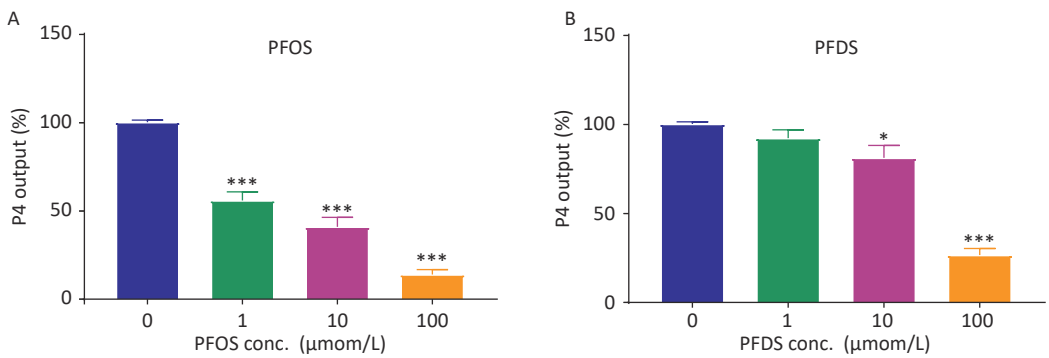

Figure 6. (A) PFOS- and (B) PFDS-mediated inhibition of P4 production by human JEG-3 cells after 24 h. means ± SD (n = 4); $^{*}P < 0.05$, $^{***}P < 0.001$ compared to control. CON, control; P4, progesterone; PFDS, perfluorodecanesulfonic acid; PFOS, perfluorooctanesulfonic acid; SD, standard deviation.

hydroxysteroid dehydrogenase 2[31]; and PFOS > PFHxS = PPFBS in inhibiting human and rat 11β-hydroxysteroid dehydrogenase 1[32]. PFOS is the most potent inhibitor of these enzymes.

Previous studies showed that some PFCA molecules, such as perfluorodecanoic acid (PFDA), PFUnA, and perfluorododecanoic acid (PFDoA), moderately inhibits rat placental *r*3β-HSD4, although they were 4–5-fold less potent to inhibit *r*3β-HSD4 than *h*3β-HSD1[16]. Surprisingly, in this study, we found that all 100 μmol/L PFSA did not affect *r*3β-HSD4 activity. Therefore, there are clear species-dependent differences between humans and rats. However, PFOS potently inhibits rat testicular *r*3β-HSD1 (IC_{50}: 1.35 μmol/L)[29], supporting the notion that PFOS specifically inhibits different 3β-HSD isoforms. We speculate that this may be due to the differences in the catalytic residue, for example, the catalytic residue Ser125 in *h*3β-HSD1 versus Thr125 in *r*3β-HSD4. Mutating Ser125 to Thr125 in *h*3β-HSD1 reduces the affinity for the inhibitor trilostane by approximately 10-fold[26,27], possibly explaining the insensitivity of *r*3β-HSD4 toward PFAS, including PFCA[16].

In this study, we showed that PFOS potentially inhibits *h*3β-HSD1 (IC_{50}: 9.03 μmol/L) and PFDS was a moderate inhibitor of this enzyme. *h*3β-HSD1 inhibition apparently suppressed P4 production in JEG-3 cell line after PFOS and PFDS treatment (Figure 6). In this study, PFSA did not inhibit human placental CYP19A1 activity, indicating that PFSA specifically inhibit *h*3β-HSD1 activity.

Apparently, PFOS inhibits *h*3β-HSD1 activity, with IC_{50} within low micromolar range. The IC_{50} of PFOS for inhibiting *h*3β-HSD1 activity (approximately 60 nmol/L) was higher than the average serum PFOS level (33.3 ng/mL) in China[7]. However, for occupational workers, the concentration of some PFAS (such as PFOS) can exceed 100 μmol/L[3,28], so people raised concerns about occupational workers.

P4 production in the human placenta is important for maintaining pregnancy. Some PFSA molecules inhibit *h*3β-HSD1 activity, possibly impairing placental function. Human studies have

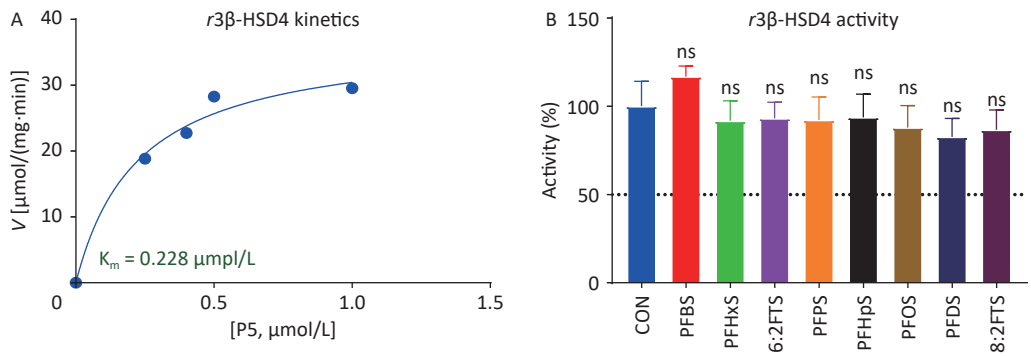

Figure 7. (A) Michaelis–Menten kinetics and (B) screening assay of perfluoroalkyl sulfonic acid to inhibit rat placental *r*3β-HSD4 activity. means ± SD (*n* = 4); No significant ("ns") difference compared to CON was observed. CON, control; *r*3β-HSD4, rat 3β-hydroxysteroid dehydrogenase 4; SD, standard deviation.

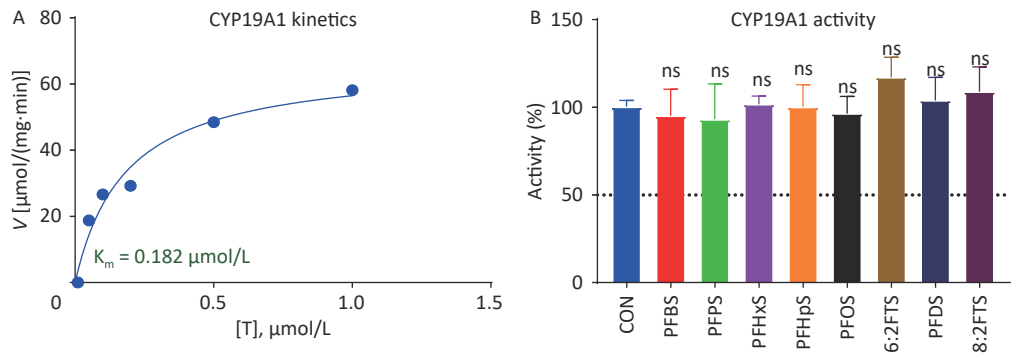

Figure 8. (A) Michaelis–Menten kinetics and (B) screening assay of PFSA to inhibit human placental CYP19A1 activity. means ± SEM (*n* = 4); No significant ("ns") difference compared to CON was observed. CON, control; CYP19A1, aromatase; PFSA, polyfluoroalkyl sulfonic acid; SEM, standard error of mean.

identified associations between PFOS, preeclampsia, and low birth weight[11-14]. Direct placental *h*3β-HSD1 inhibition by PFOS may also cause these adverse effects. However, data from direct inhibition studies and human cell lines should be extrapolated cautiously.

In conclusion, this study demonstrated the structure-dependent PFSA-mediated inhibition of human *h*3β-HSD1 activity. The inhibitory potency of PFSA was in the order PFOS > PFDS > PFHpS > PFBS = PFPS = PFHxS = PFDoS = 6:2FTS = 8:2FTS, and an adequate molecule size and functional group (sulfonic acid) of PFSA were critical for the inhibition of *h*3β-HSD1 activity. PFOS is the most potent inhibitor of human *h*3β-HSD1 among PFSA.

AUTHOR'S CONTRIBUTION

The authors declare no conflicts of interest. L.T., B. M., and B.Z. designed the study, analyzed the data, and wrote the manuscript. J. L. and Y.T. conducted the study. H.L. helped with the design and docking analysis. R.G. helped with the design, editing, and funding.

Received: November 26, 2022;
Accepted: February 24, 2023

REFERENCES

1. Mokra K. Endocrine disruptor potential of short- and long-chain perfluoroalkyl substances (PFASs)-a synthesis of current knowledge with proposal of molecular mechanism. Int J Mol Sci, 2021; 22, 2148.
2. Abdellatif AG, Préat V, Vamecq J, et al. Peroxisome proliferation and modulation of rat liver carcinogenesis by 2, 4-dichlorophenoxyacetic acid, 2, 4, 5-trichlorophenoxyacetic acid, perfluorooctanoic acid and nafenopin. Carcinogenesis, 1990; 11, 1899−902.
3. Jensen AA, Leffers H. Emerging endocrine disrupters: perfluoroalkylated substances. Int J Androl, 2008; 31, 161−9.
4. Johnson JD, Gibson SJ, Ober RE. Cholestyramine-enhanced fecal elimination of carbon-14 in rats after administration of ammonium [^{14}C]perfluorooctanoate or potassium [^{14}C]perfluorooctanesulfonate. Fundam Appl Toxicol, 1984; 4, 972−6.
5. Giesy JP, Kannan K. Peer Reviewed: Perfluorochemical surfactants in the environment. Environ Sci Technol, 2002; 36, 146A−52A.
6. Olsen GW, Mair DC, Church TR, et al. Decline in perfluorooctanesulfonate and other polyfluoroalkyl chemicals in American Red Cross adult blood donors, 2000-2006. Environ Sci Technol, 2008; 42, 4989−95.
7. Zhang YF, Beesoon S, Zhu LY, et al. Isomers of perfluorooctanesulfonate and perfluorooctanoate and total perfluoroalkyl acids in human serum from two cities in North China. Environ Int, 2013; 53, 9−17.
8. Olsen GW, Burris JM, Ehresman DJ, et al. Half-life of serum elimination of perfluorooctanesulfonate, perfluorohexanesulfonate, and perfluorooctanoate in retired fluorochemical production workers. Environ Health Perspect, 2007; 115, 1298−305.
9. U. S. EPA. Draft risk assessment of the potential human health effects associated with exposure to perfluorooctanoic acid and its salts. Washington: U. S. Environmental Protection Agency, 2005.
10. Chengelis CP, Kirkpatrick JB, Myers NR, et al. Comparison of the toxicokinetic behavior of perfluorohexanoic acid (PFHxA) and nonafluorobutane-1-sulfonic acid (PFBS) in cynomolgus monkeys and rats. Reprod Toxicol, 2009; 27, 400−6.
11. Stein CR, Savitz DA, Dougan M. Serum levels of perfluorooctanoic acid and perfluorooctane sulfonate and pregnancy outcome. Am J Epidemiol, 2009; 170, 837−46.
12. Betts K. PFOS and PFOA in humans: new study links prenatal exposure to lower birth weight. Environ Health Perspect, 2007; 115, A550.
13. Apelberg BJ, Witter FR, Herbstman JB, et al. Cord serum concentrations of perfluorooctane sulfonate (PFOS) and perfluorooctanoate (PFOA) in relation to weight and size at birth. Environ Health Perspect, 2007; 115, 1670−6.
14. Fei CY, McLaughlin JK, Tarone RE, et al. Perfluorinated chemicals and fetal growth: a study within the Danish National Birth Cohort. Environ Health Perspect, 2007; 115, 1677−82.
15. Simard J, Ricketts ML, Gingras S, et al. Molecular biology of the 3β-hydroxysteroid dehydrogenase/Δ^5-Δ^4 isomerase gene family. Endocr Rev, 2005; 26, 525−82.
16. Wang SW, Zhang BR, Zhai YN, et al. Structure-activity relationship analysis of perfluoroalkyl carbonic acids on human and rat placental 3β-hydroxysteroid dehydrogenase activity. Toxicology, 2022; 480, 153334.
17. Jiang B, Kamat A, Mendelson CR. Hypoxia prevents induction of aromatase expression in human trophoblast cells in culture: potential inhibitory role of the hypoxia-inducible transcription factor Mash-2 (mammalian achaete-scute homologue ous protein-2). Mol Endocrinol, 2000; 14, 1661−73.
18. Rainey WE, Rehman KS, Carr BR. The human fetal adrenal: making adrenal androgens for placental estrogens. Semin Reprod Med, 2004; 22, 327−36.
19. Samson M, Labrie F, Luu-The V. Specific estradiol biosynthetic pathway in choriocarcinoma (JEG-3) cell line. J Steroid Biochem Mol Biol, 2009; 116, 154−9.
20. Albrecht ED, Pepe GJ. Estrogen regulation of placental angiogenesis and fetal ovarian development during primate pregnancy. Int J Dev Biol, 2010; 54, 397−408.
21. Xu RA, Mao BP, Li SL, et al. Structure-activity relationships of phthalates in inhibition of human placental 3β-hydroxysteroid dehydrogenase 1 and aromatase. Reprod Toxicol, 2016; 61, 151−61.
22. Jumper J, Evans R, Pritzel A, et al. Highly accurate protein structure prediction with AlphaFold. Nature, 2021; 596, 583−9.
23. Varadi M, Anyango S, Deshpande M, et al. AlphaFold protein structure database: massively expanding the structural coverage of protein-sequence space with high-accuracy models. Nucleic Acids Res, 2022; 50, D439−44.
24. Grosdidier A, Zoete V, Michielin O. SwissDock, a protein-small molecule docking web service based on EADock DSS. Nucleic Acids Res, 2011; 39, W270−7.
25. Wallace AC, Laskowski RA, Thornton JM. LIGPLOT: a program to generate schematic diagrams of protein-ligand interactions. Protein Eng Des Sel, 1995; 8, 127−34.
26. Thomas JL, Mason JI, Brandt S, et al. Structure/function relationships responsible for the kinetic differences between human type 1 and type 2 3β-hydroxysteroid dehydrogenase and for the catalysis of the type 1 activity. J Biol Chem, 2002;

277, 42795−801.
27. Thomas JL, Duax WL, Addlagatta A, et al. Serine 124 completes the Tyr, Lys and Ser triad responsible for the catalysis of human type 1 3β-hydroxysteroid dehydrogenase. J Mol Endocrinol, 2004; 33, 253−61.
28. Hekster FM, De Voogt P, Pijnenburg AMCM, et al. Perfluoroalkylated substances: aquatic environmental assessment. Assen: Rijkswaterstaat, 2002: 99.
29. Zhao BH, Hu GX, Chu YH, et al. Inhibition of human and rat 3β-hydroxysteroid dehydrogenase and 17β-hydroxysteroid dehydrogenase 3 activities by perfluoroalkylated substances. Chem Biol Interact, 2010; 188, 38−43.
30. Doi M, Takahashi Y, Komatsu R, et al. Salt-sensitive hypertension in circadian clock-deficient *Cry*-null mice involves dysregulated adrenal Hsd3b6. Nat Med, 2010; 16, 67−74.
31. Zhao BH, Lian QQ, Chu YH, et al. The inhibition of human and rat 11β-hydroxysteroid dehydrogenase 2 by perfluoroalkylated substances. J Steroid Biochem Mol Biol, 2011; 125, 143−7.
32. Ye LP, Zhao BH, Cai XH, et al. The inhibitory effects of perfluoroalkyl substances on human and rat 11β-hydroxysteroid dehydrogenase. Chem Biol Interact, 2012; 195, 114−8.